Journal of Materials Science & Technology 81 (2021) 43–50

Contents lists available at ScienceDirect

Journal of Materials Science & Technology

journal homepage: www.jmst.org

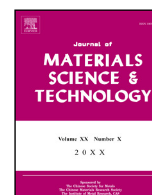

Ultrathin, flexible, and high-strength Ni/Cu/metallic glass/Cu/Ni composite with alternate magneto-electric structures for electromagnetic shielding

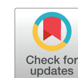

Zenan Ma [a,b], Jiawei Li [b,*], Jijun Zhang [c], Aina He [b], Yaqiang Dong [b], Guoguo Tan [b], Mingqiang Ning [b], Qikui Man [b], Xincai Liu [a,*]

[a] Faculty of Materials Science and Chemical Engineering, Ningbo University, Ningbo, 315211, China
[b] CAS Key Laboratory of Magnetic Materials and Devices, and Zhejiang Province Key Laboratory of Magnetic Materials and Application Technology, Ningbo Institute of Materials Technology & Engineering, Chinese Academy of Sciences, Ningbo, 315201, China
[c] Institute of Fundamental and Frontier Sciences, University of Electronic Science and Technology of China, Chengdu, 610054, China

ARTICLE INFO

Article history:
Received 9 October 2020
Received in revised form
17 November 2020
Accepted 10 December 2020
Available online 9 January 2021

Keywords:
Electromagnetic shielding
Thermal management
Mechanical properties
Fe-based metallic glasses
Alternate magnetic and electrical structures

ABSTRACT

Electromagnetic interference (EMI) shielding materials with ultrathin, flexible, superior mechanical and thermal management properties are highly desirable for smart and wearable electronics. Here, ultrathin and flexible Ni/Cu/metallic glass/Cu/Ni (Ni/Cu/MG) multilayer composite with alternate magnetic and electrical structures was designed via facial electroless plating of Cu and Ni on an Fe-based metallic glass. The resultant 0.02 mm-thick Ni/Cu/MG composite displays a superior EMI shielding effectiveness (EMI SE) of 35 dB and a great EMI SE/t of 1750 dB/mm, which is greater than those of composites with monotonous multilayer or homogeneous structures. The improved EMI SE originates from the massive ohmic losses, the enhanced internal reflection/absorption, and the abundant interfacial polarization loss. Particularly, Ni/Cu/MG exhibits a high tensile strength of up to 1.2 GPa and outstanding mechanical stability, enabling the EMI SE remains unchanged after 10,000 times of bending. Moreover, Ni/Cu/MG has excellent Joule heating characteristics and thermal stability, which is very suitable for heating components of wearable hyperthermia devices.

© 2021 Published by Elsevier Ltd on behalf of The editorial office of Journal of Materials Science & Technology.

1. Introduction

Modern electronic devices, such as mobile phones, computers and wearable electronics, have been developing toward miniaturization, integration, high-frequency and multifunction, thus causing more and more serious electromagnetic interference (EMI) problems. Highly efficient EMI shielding and thermal management materials are essential for smart and wearable electronics, especially if they can be thin, flexible, mechanically strong, and easy to fabricate [1–6]. Conductive polymer composites (CPCs) composed of polymer and high conductive fillers such as carbon materials (nano-tube [7], carbon fiber [8], graphene [9], etc.), metal nanoparticles and nanowires (silver [10], copper [4], nickel [11], etc.) have been widely studied owing to their high conductivity, flexibility, corrosion resistance and lightweight. However, CPCs have poor mechanical and thermal durability, and usually require high conductive fillers and large thickness to achieve acceptable EMI shielding effectiveness (EMI SE) [6,12]. 2D MXenes with unique spatial structure and high conductivity exhibit exceptional EMI SE (75-116 dB) at ultrathin thickness (0.01–0.04 mm), which occupies a leading position in lightweight shielding materials [2,13,14]. However, MXenes are far from practical application owing to their difficulties in preparation, weak interface adhesion with polymers and limited theoretical and experimental research [14].

Traditional metals and their composites are the most widely used EMI shielding materials owing to their excellent conductivity and soft magnetic properties. Yet, the high specific weight, poor flexibility and hard processing of metal-based materials limit their application in smart and wearable electronics [6]. Electroless plating a uniform and thin metal coating on a flexible substrate has been reported as an effective method to solve the above problems. For instance, Li et al. [15] prepared flexible composite materials by simply electroless plating 500 nm Ni on nylon mesh and then mixed with polypropylene, which depicts an EMI SE of 50.6 dB. Li et al. [16]

* Corresponding authors.
E-mail addresses: lijw@nimte.ac.cn (J. Li), liuxincai@nbu.edu.cn (X. Liu).

https://doi.org/10.1016/j.jmst.2020.12.012
1005-0302/© 2021 Published by Elsevier Ltd on behalf of The editorial office of Journal of Materials Science & Technology.

prepared a MWCNT/Ni@CLF/PEEK flexible composite with an EMI SE of 48.1 dB by electroless plating Ni. Xu et al. [17] used electroless Ag-plated melamine foam and multi-walled carbon nanotubes as the skeleton to prepare a lightweight epoxy composite foam with an EMI SE of 68 dB. In addition, electroless Ag plating on polymer or cotton fibers can also obtain composites with lightweight, flexibility and high EMI SE [18,19]. Nevertheless, the composites obtained by electroless plating a uniform conductive metal on a flexible polymer matrix have low strength, unsatisfactory thermal management performance and poor bending stability caused by the thick coating and the mismatch of the Young's modulus and thermal expansion coefficient between the coating and the substrate [3]. To solve these problems. Zhang et al. [3] obtained an electromagnetic shielding composite with flexibility, good mechanical and corrosion durability via electroless plating ultrathin NiCuP coatings on an FeSiB metallic glass. However, the uneven heat conduction of the five-layer electroless-plated composite bonded by double-sided tapes reduces its thermal management performance. In addition, the monotonous layered structure requires a large thickness to obtain high shielding performance, which increases cost and processing difficulty.

It is known that the fix impedance mismatch between interfaces caused by uniform or simple structures is difficult to dissipate electromagnetic waves (EMWs) effectively. Recent studies have shown that absorption-dominated EMI shielding can be achieved through a reasonable design of magnetic/electric gradient structures owing to the enhanced multiple absorption/reflection and interfacial polarization losses [20–23]. Sheng et al. [23] designed Fe_3O_4@rGO/MWCNT/WPU composites with an electro-magnetic gradient structure, which displays an EMI SE of 35.9 dB and reduced power coefficient of reflectivity (0.27). Yang et al. [22] prepared lightweight silicone rubber/Ag@HGMs/Fe_3O_4@MWCNTs composite foams with gradient structure, revealing an EMI SE of 30.5 dB at a thickness of 0.7 mm. Moreover, it has been reported that constructing a large number of interfaces to enhance the interface polarization effect is more conducive to realize the optimization of EMI SE [24–26]. However, most of the work only uses electrical performance without introducing magnetic loss, thus the material is thick, which is not conducive to miniaturization. In addition, the complicated preparation process also limits their applications. Therefore, by tuning impendence mismatch degree with controllable arrangement of magnetic and electrical metal coatings, the design of alternate absorption and reflection shielding structure would provide a strategy for fabricating metal-based composites with high EMI SE, lightweight and flexibility.

In this work, we fabricated an ultrathin and flexible Ni/Cu/metallic glass/Cu/Ni (Ni/Cu/MG) multilayer composite with highly efficient EMI SE, superior mechanical and thermal management performance. The alternate magneto-electric structures constructed by electroless plating Ni and Cu on a soft magnetic FeSiBNbCu metallic glass ribbon provide a multiple absorption and reflection network, thereby achieving an EMI SE of 35 dB at a thickness of only 0.02 mm. Moreover, the Ni/Cu/MG composite displays great tensile strength of 1.2 GPa, sufficient conductive reliability and mechanical stability upon 10,000 bending cycles. In addition, satisfactory Joule heating temperature under low supply voltage, good thermal stability and rapid response time make it suitable for wearable thermotherapy.

2. Experimental

2.1. Materials

$Fe_{76}Si_{13}B_8Nb_2Cu_1$ metallic glass ribbons (B plus Co. Ltd.) with a width of 60 mm and thickness of approximately 17 μm were used as substrates for electroless plating due to their excellent mechanical properties and thermal stability. Stannous chloride ($SnCl_2$), palladium chloride ($PbCl_2$), nickel sulfate ($NiSO_4{\cdot}6H_2O$), copper sulfate pentahydrate ($CuSO_4{\cdot}5H_2O$), sodium acetate trihydrate ($NaC_2H_3O_2{\cdot}3H_2O$), trisodium citrate dihydrate ($Na_3C_6H_5O_7{\cdot}2H_2O$), sodium hypophosphite ($NaH_2PO_2{\cdot}H_2O$), thiourea (CH_4N_2S), Lactic acid ($C_3H_6O_3$), and hydrochloric acid (HCl, 36 wt.%-38 wt.%) (National Medicine Group Chemical Reagent Co., Ltd) were used in electroless plating.

2.2. Synthesis of Cu/MG, Ni/MG, Ni/Cu/MG composites

The Ni/MG, Cu/MG, and Ni/Cu/MG composites were fabricated by electroless plating Ni and Cu on the surface of $Fe_{76}Si_{13}B_8Nb_2Cu_1$ MG ribbons. Electroless plating was accomplished through sensitization, activation, chemical deposition and subsequent cleaning and drying, as described schematically in Fig. 1(a). The sensitization process was to place the ribbons in a solution of 10 g/L $SnCl_2$ and 40 mL/L 38 % HCl at 25 °C for 3 min. Secondly, the sensitized ribbons were washed with deionized water and then placed in a solution containing 0.5 g/L $PbCl_2$, 10 mL/L 38 % HCl at 25 °C for 3 min to complete the activation process. Thirdly, the activated ribbons were rinsed with deionized water to clean the solution attached to the surface of the samples, and then were divided into three groups for subsequent chemical deposition. Fourthly, according to the optimal process conditions explored in the preliminary experiments (Fig. S1), one group was immersed in the solution of $NiSO_4$ (20 g/L) at 90 °C for 3 min, and mechanically stirred to obtain Ni/MG. The other two groups were immersed in the solution of $CuSO_4$ at 90 °C for 9 min, and mechanically stirred to obtain Cu/MG. After Cu/MG were sensitized and activated again, they were placed in the solution of $NiSO_4$ (20 g/L) at 90 °C for 3 min and mechanically stirred to obtain Ni/Cu/MG (Fig. 1(a)). Finally, all samples were rinsed with ethanol and dried in the air.

2.3. Material characterization and measurements

Field-emission scanning electron microscope (SEM FEI Quanta FEG 250) was used to characterize the surface and interface morphology of the composites. Elemental composition analysis was performed using energy dispersive spectroscopy (EDS). The microstructure and selected area electron diffraction (SAED) were characterized by a high-resolution transmission electron microscope (HRTEM Talos F200x). The TEM samples were prepared by FIB (Helios-G4-CX). Vibration sample magnetometer (VSM Lakeshore 7410) was used to obtain saturation magnetization. The conductivity was obtained by the four-probe method on the Napson Cresbox (CRESBOX) measurement system. The EMI SE was measured using a vector network analyzer (VNA Agilent N5234A) at room temperature with a frequency band of 8−12 GHz. The composites were cut into a size of approximately 22.86×10.16 mm^2 in order to adaptive the waveguide fixture port. Infrared thermal imaging camera (FLIR A325sc) was used to record temperature changes during heating and cooling. Tensile test was carried out on an electronic universal testing machine (Zwick Z030TE, Germany) at a tensile rate of 10^{-4} m/s. The software used for numerical simulation was Computer Simulation Technology (CST) Microwave Studio. The antenna module was selected, and a multilayer structure model similar to the experiment was established. The background was vacuum, and the two ports were distributed at 75 mm on both sides of the sample to construct a waveguide model. The frequency domain solver was used to solve the transmission coefficient to obtain power flow intensity distribution.

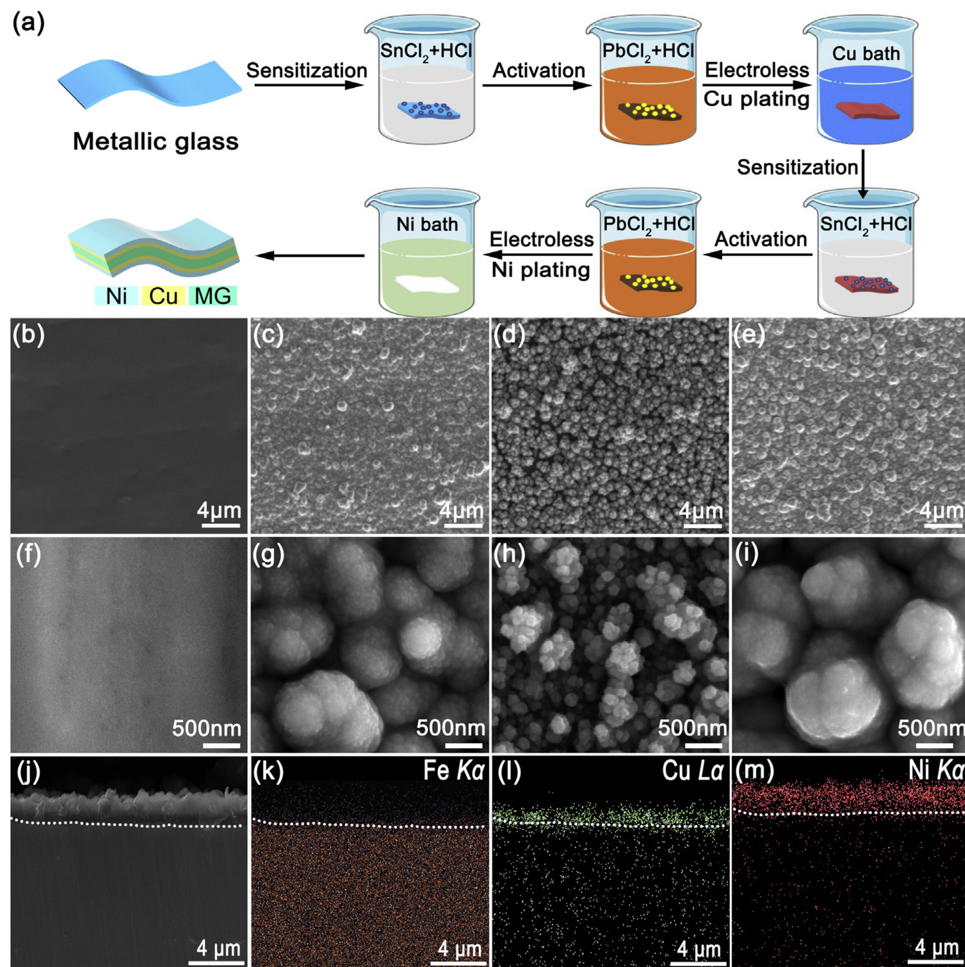

Fig. 1. Fabrication and characterization of Ni/Cu/MG. (a) Schematic fabricating process and illustration. (b-e) Surface morphologies of MG, Ni/MG, Cu/MG and Ni/Cu/MG, respectively. (f-i) Enlarged images of (b-e). (j) Cross-sectional image. (k-m) Elemental distribution images.

3. Results and discussion

3.1. Microstructure of Ni/Cu/MG multilayer composite

The broad diffuse X-ray curve without any sharp peak (Fig. S2) confirms the amorphous structure of MG. After electroless plating, the diffraction peaks of Ni and Cu can be clearly observed on the broad diffuse peak of MG, indicating that Ni/MG, Cu/MG and Ni/Cu/MG multilayer structures were successfully constructed. In order to characterize the morphologies and structures of the composites, field-emission SEM was employed. The pristine MG displays a smooth surface, whereas all electroless plated samples display nacre-like rough surface; neither cracks nor pores were observed on the surfaces (Fig. 1(b)-(e)). The nacre-like antenna structure can be further illustrated by local surface magnification (Fig. 1(f)-(i)). Fig. 1(j)-(m) depict the cross-sectional morphology and element distribution of Ni/Cu/MG, respectively. Elemental mappings further confirm the existence of Ni and Cu multilayer structure. The Ni coating with a thickness of approximately 1 μm and the Cu coating with a thickness of approximately 0.5 μm are uniformly distributed on the surface of the MG substrate from top to bottom. Thus, the total thickness of Ni/Cu/MG is approximate 0.02 mm. It is worth noting that owing to the diffusion of elements, a transition layer could be formed between the interfaces, which not only helps to improve the bonding strength between the layers, but also builds a magnetic-electro gradient structure. TEM results (Figs. 2 and S3) further confirm the existence of interdiffusion between the layers and the substrate. Embedded Cu can be found in both the MG substrate and the Ni layer. The SAED (Fig. 2(a)) and high-resolution images (Fig. 2(b)) indicate the multilayer structure consists of NiP (100), Ni (100), Cu (100) and Cu (111), which is consistent with the XRD results. As schematically illustrated in Fig. 1(a), Ni/Cu/MG is composed of two Ni magnetic layers (Fig. S4), two Cu conductive layers and a metallic glass layer with high magnetic permeability, thereby constructing four magnetic and electrical mismatched interfaces inside the material.

3.2. Electrical and magnetic properties of Ni/Cu/MG

Fig. 3(a) shows the electrical conductivity of MG, Ni/MG, Cu/MG and Ni/Cu/MG. The pristine MG exhibits low conductivity due to its unique disordered structure. The conductivity of Ni/MG is almost the same as that of MG, whereas the ultrathin Cu layers increase the conductivity of MG by 12 %. Interestingly, after electroless Ni and Cu plating, the conductivity of Ni/Cu/MG reaches 6.5×10^5 S/m (135330 S/m greater than that of MG). The significant increment in conductivity is due to the corrosion-resistant Ni layers can effectively prevent the oxidation of the Cu layers [27]. As we all know, the higher the conductivity of the material,

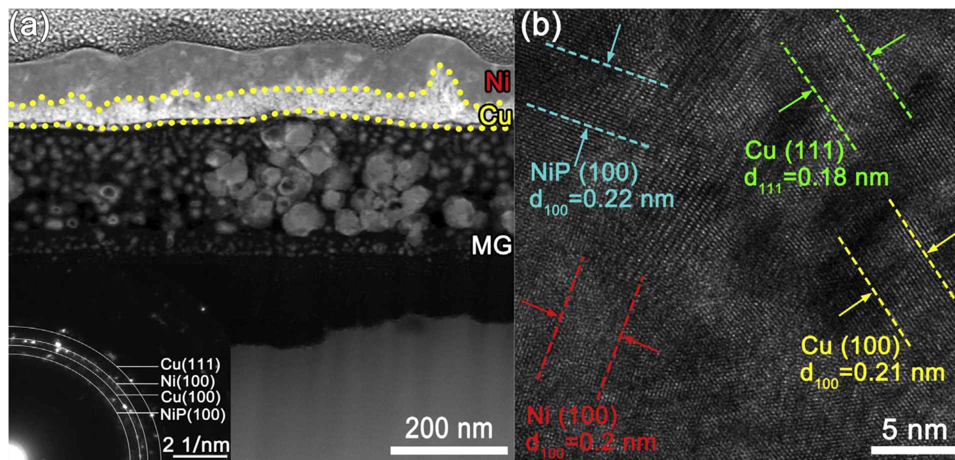

Fig. 2. TEM microstructure of Ni/Cu/MG. (a) Cross-sectional bright-field image. The inset in (a) shows the SAED pattern. (b) HRTEM image, indicating the interdiffusion of Ni, Cu and MG.

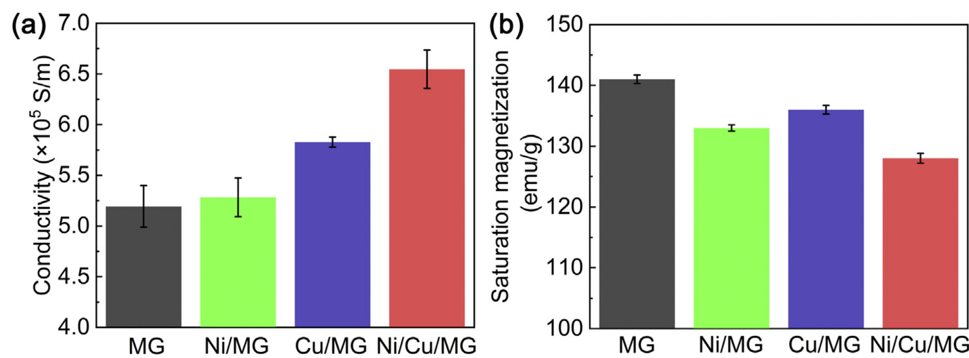

Fig. 3. Electrical and magnetic properties of MG, Ni/MG, Cu/MG and Ni/Cu/MG. (a) Electrical conductivity. (b) Saturation magnetization.

the better the EMI shielding performance. Moreover, the different conductivity of each layer of the composite undoubtedly generates multiple conductive gradient structure at internal interfaces, which is also beneficial for shielding EMWs [20]. Therefore, electroless Cu plating would effectively improve the EMI SE of MG, and Ni/Cu/MG with the highest conductivity may have the best shielding performance. In addition, the inherent magnetic property of a material is also a factor that affects EMI SE. Fig. S5 displays the *M-H* hysteresis loops of MG, Ni/MG, Cu/MG and Ni/Cu/MG at room temperature. All samples display a slender hysteresis loop, indicative of their excellent soft magnetic performance such as low coercivity and high permeability. As shown in Fig. 3(b), the saturation magnetization of MG, Ni/MG, Cu/MG, and Ni/Cu/MG are 141, 133, 136, and 128 emu/g, respectively. The slight deterioration in saturation magnetization is caused by the introduction of diamagnetic Cu and slightly weaker magnetic Ni layers. Although Ni is magnetic, its saturation magnetization is lower than that of MG. Therefore, the introduction of Cu and Ni would dilute the magnetic moment of MG, so that the saturation magnetization of Ni/MG and Cu/MG is lower than that of MG. In addition, because the Ni layer is thicker than the Cu layer, the magnetic properties of Ni/MG are inferior to that of Cu/MG. Although the saturation magnetization of electroless plated samples is slightly lower than that of MG, the change in magnetic properties is very small. In addition, it has been reported that the alternate magnetism inside the multilayer structure has a positive effect on absorbing EMWs [22,23]. Therefore, the enhanced electrical conductivity and alternating magnetic and electrical structures may significantly improve the electromagnetic shielding performance of MG.

3.3. Electromagnetic shielding performance and mechanism

EMI SE is an important index to evaluate the attenuation capability of a material to EMWs. The EMI SE can be expressed as [3,28]:

$$SE_T = SE_A + SE_R + SE_M \quad (1)$$

where SE_T, SE_A, SE_R and SE_M represent the total, absorption, reflection and multiple reflection loss, respectively. In general, when SE_T is greater than 20 dB or SE_A is greater than 15 dB, SE_M can be ignored. At this time, SE_T is simplified to the sum of SE_A and SE_R [29]. SE_T, SE_R and SE_A can be expressed as:

$$SE_T=10\log(1/|S_{21}|)^2 \quad (2)$$

$$SE_A=10\log(1-\left|S_{11}\right|^2/\left|S_{21}\right|^2) \quad (3)$$

$$SE_R=10\log(1/1-\left|S_{21}\right|^2) \quad (4)$$

where, S_{21} and S_{11} can be measured by vector network analyzer.

Fig. 4(a) displays the total EMI SE of MG, Ni/MG, Cu/MG and Ni/Cu/MG. The EMI SE of MG is only 10 dB, which is not up to the commercial standard of 20 dB [7] and thus not suitable for high-frequency EMI shielding. After electroless Cu and Ni plating, the EMI SE of Ni/Cu/MG is increased to 35 dB, which is three times greater than that of MG. In addition, even if the coating thickness of Ni/MG and Cu/MG continuously increases until the coating peels off, their EMI shielding performance is inferior to that of Ni/Cu/MG (Figs. S1 and S6). The SE_T, SE_A, and SE_R values at 10 GHz are displayed in Fig. 4(b). A transition from the reflection-dominated to the absorption-dominated shielding mechanism can be clearly observed. The EMI SE of MG mainly comes from the

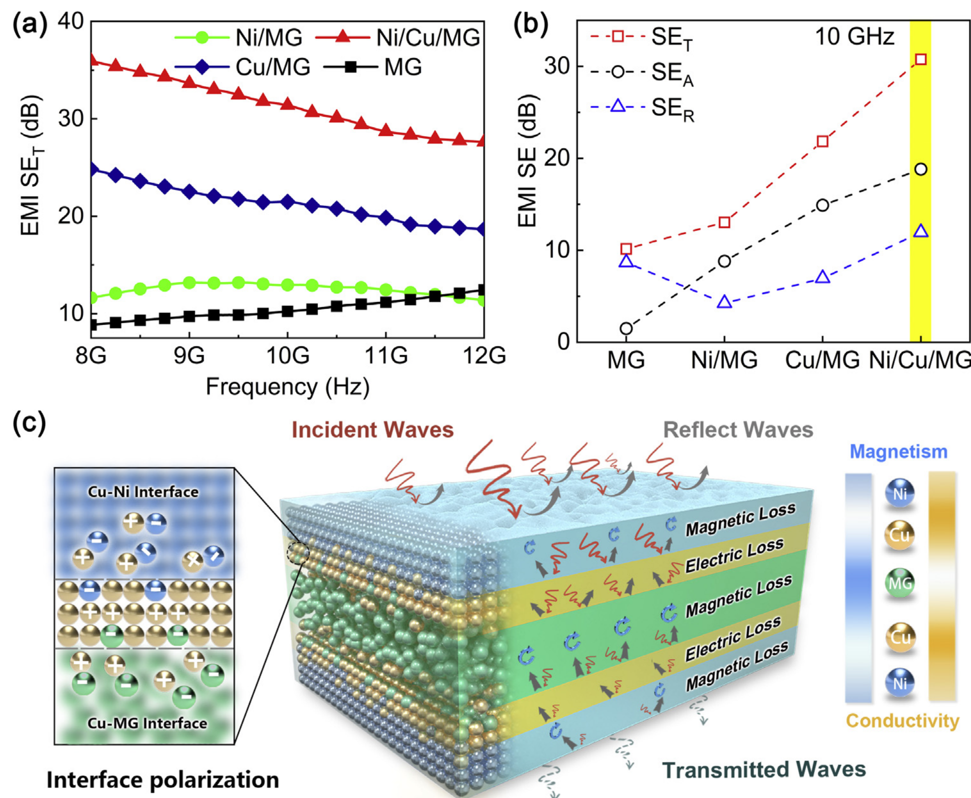

Fig. 4. (a) EMI SE and (b) SE_T, SE_A and SE_R of MG, Ni/MG, Cu/MG and Ni/Cu/MG. The dash lines are guides for eyes. (c) EMI shielding mechanism of Ni/Cu/MG.

contribution of SE_R, which is consistent with the mechanism that metal with a smooth surface mainly reflects EMWs [30]. Conversely, the primary shielding mechanism of the electroless plated MGs is absorption. Electroless Ni plating and Cu plating have little effect on the SE_R of MG, but can significantly increase its SE_A. In particular, Ni/Cu/MG has the greatest SE_A, making it have the best shielding performance. The increase in SE_A of Ni/Cu/MG can be attributed to the following aspects: first, SE_R is directly proportional to the conductivity of a shield since higher free charge carriers would increase the impedance mismatching between the air and the shield, and thus increase the reflection of EMWs [11,31,32]. As mentioned above, the Ni layer has little effect on the conductivity of MG, but it roughens the surface of MG and produces a large number of nacre-like grain structures, which is beneficial to attract EMWs into the interior of Ni/Cu/MG instead of reflecting back [3,33]. Second, Ni/Cu/MG has a more complete conductive path than other samples owing to the insertion of highly conductive Cu sandwich layers [34–37], which increases the ohmic loss [13]. Moreover, a large quantity of Cu nanoparticles embedded in the Ni and MG layers increase the contact area of the interfaces and edges, inducing more heterointerfaces and the asymmetric distribution of the charge density, thereby enhancing the interface polarization relaxation loss when the dipoles rotate directionally toward the alternating EMWs [23,38–41]. Third, the multilayer structure increases the path of EMWs before penetrating the composite and enhances the interaction between EMWs and interfaces, leading to the increase in absorption loss [13]. Particularly, the alternate magnetic and electrical structures form magnetic and conductive gradient near the interfaces, which promotes absorption through strong hysteresis and dielectric losses [20–23,42].

Fig. 4(c) schematically illustrates the EMI shielding mechanism of Ni/Cu/MG. As EMWs strike the surface of Ni/Cu/MG with a great number of nacre-like Ni nanoparticles, some EMWs are directly reflected under the competition of impedance mismatch and rough surface structure, and some incident EMWs are absorbed by the magnetic Ni layer [43]. Immediately after contacting the Cu layer with high conductivity and abundant nacre-like nanostructure, the incoming EMWs interact with the high-density electrons and dipoles induced by plentiful heterointerfaces and edges, resulting in massive ohmic losses and polarization relaxation loss to dissipate the EMWs. The surviving EMWs encounter the Cu-MG interface with a larger difference in magnetic and electrical properties, leading to stronger dielectric loss owing to the enhanced interfacial polarization relaxation [44–47]. Then, the transmitted EMWs enter the thick MG magnetic layer, and are further absorbed through hysteresis loss, natural resonance, exchange resonance, and eddy current effect [31,48]. As the EMWs meet the Cu layer again, they are further reflected back into the matrix owing to the high dielectric loss of the Cu layer, and the interaction between EMWs and the Cu-MG interface repeats. The residual EMWs with little energy undergo the same absorption process when they enter the next Ni layer. In addition, the multilayer structure forces EMWs to reflect back and forth between these layers, promoting the dissipation and attenuation of EMWs until completely absorbed. Consequently, the alternate two Ni/Cu and two Cu/MG interfaces with different magnetic and electrical properties significantly enhance the electric loss, magnetic loss, and interfacial polarization loss, thereby improving the overall EMI SE of Ni/Cu/MG.

3.4. Simulation of power flow

We adopted CST calculations to simulate the electromagnetic energy distribution when EMWs pass through Ni/Cu/MG, Cu/MG and Ni/MG with the same thickness to verify the advantages of the multilayer alternate magnetic and electrical structures in shielding EMWs. For Ni/Cu/MG (Fig. 5(a)), some EMWs are dispersed when passing through the Ni layer. After entering the Cu layer, most of the transmitted EMWs are attenuated, and then almost completely

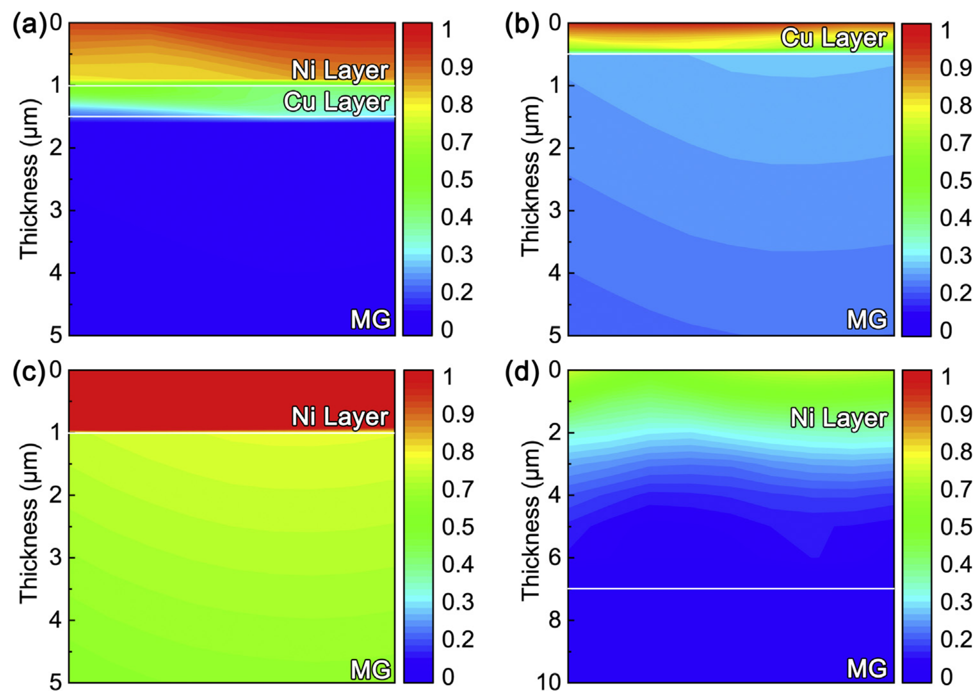

Fig. 5. Power flow intensity distribution map. (a) Ni/Cu/MG. (b) Cu/MG. (c, d) Ni/MG with electroless Ni plating for 3 min and 7 min, respectively. All the power flow intensity is normalized, and the color from red to blue represents the EMWs vary from strong to weak.

disappear in the MG layer. For Cu/MG (Fig. 5(b)), the power flow intensity significantly decreases after the EMWs penetrate the Cu layer. However, the MG layer cannot effectively absorb the remaining EMWs, indicating that the shielding performance of a single Cu plating structure is not satisfactory. For Ni/MG (Fig. 5(c)), the Ni and MG layers have a limit effect on the incoming EMWs due to the insufficient conductivity and the monotonous structure. In order to efficiently attenuate the EMWs, the thickness of the Ni layer of Ni/MG needs to be more than 7 μm, as shown in Fig. 5(d). Unfortunately, the increased thickness would significantly deteriorate the mechanical flexibility and stability of Ni/MG (Figs. S1 and S6). Consequently, the simulation results are consistent with the experimental results, confirming that the designed Ni/Cu/MG composite with a multilayer alternate magnetic and electrical structure can achieve excellent EMI shielding performance under ultrathin thickness.

3.5. Mechanical and thermal management performance

In practical applications of smart and wearable electronics, it is very important to evaluate the durability of Ni/Cu/MG under mechanical bending. After 10,000 times of repeated bending at an angle of nearly 180 degrees, the EMI SE has no obvious deterioration (Fig. S7(a)), and no cracks and shedding on the coating were found, indicating the excellent mechanical stability of Ni/Cu/MG. Moreover, the tape test indicates that Ni/Cu/MG displays good bonding strength between the coatings and the MG substrate (Fig. S7(b)), which may be due to the ultrathin and dense coating structure and the gradient interfaces caused by element diffusion (Figs. 1, 2 and S3). Further, all samples have excellent tensile strength exceeding 1100 MPa (Fig. 6(a)). The slight decrease in the tensile strength of the electroless plated MGs may be related to the slight corrosion on the surface of MG during the electroless plating process. As shown in Fig. S8, a large number of pitting pits are generated on the material surface after the sensitization process. Although these pitting pits provide the binding sites of active sites for the subsequent activation process, they also become part of stress concentration. Similarly, after the activation process, the uneven distribution of active sites leads to more point defects, which in turn leads to a decrease in the overall tensile strength of MG [49]. Nevertheless, the tensile strength of Ni/Cu/MG is still much higher than most EMI shielding materials such as metals, MXenes, and CPCs doped with carbon and nanometer metal materials. Besides, the thickness-reduced EMI SE, EMI SE/t, is a highly valuable parameter to evaluate the shielding performance of different shields when considering a material's thickness. Thus, the superiority of the ultrathin, flexible, and high-strength Ni/Cu/MG composite over other shielding materials are highlighted by comparing their EMI SE/t and tensile strength with literature data. As shown in Fig. 6(b) and Table S1, Ni/Cu/MG exhibits a great tensile strength of 1220 MPa and high EMI SE/t up to 1750 dB/mm. Compared with other shielding materials, it is ranked at the top of the comparison chart. The results are exciting because several commercial requirements are simultaneously concentrated in one shielding material, such as excellent EMI shielding performance, ultrathin, flexibility, outstanding mechanical strength and stability, and easy to fabricate.

Moreover, Ni/Cu/MG has great potential as a high-performance Joule heating element in smart and wearable flexible devices. Fig. 7(a) displays the surface temperature of Ni/Cu/MG as a function of time and applied voltage. At the low applied voltage of 0.1 V, the temperature of Ni/Cu/MG rises from room temperature to 41 °C, reaching the appropriate temperature for wearable hyperthermia to maintain warmth or relieve pain and discomfort [35,50]. A small increase in applied voltage can make Ni/Cu/MG quickly reach a stable temperature owing to the higher Joule heat caused by the higher current. Taking into account the heat exchange and heat loss in practical applications, the ideal temperature of heating components is 60–70 °C [51,52]. It can be seen that when the power supply voltage is 0.2 V, Ni/Cu/MG reaches 64 °C within 6 s, and the temperature is uniformly distributed and remains stable within 1 h (Fig. 7(c)). This is because MG has a small temperature coefficient of resistivity and uniform microstructure (Fig. 7(b)), which avoids heating localization [53], and the internal heat could be quickly

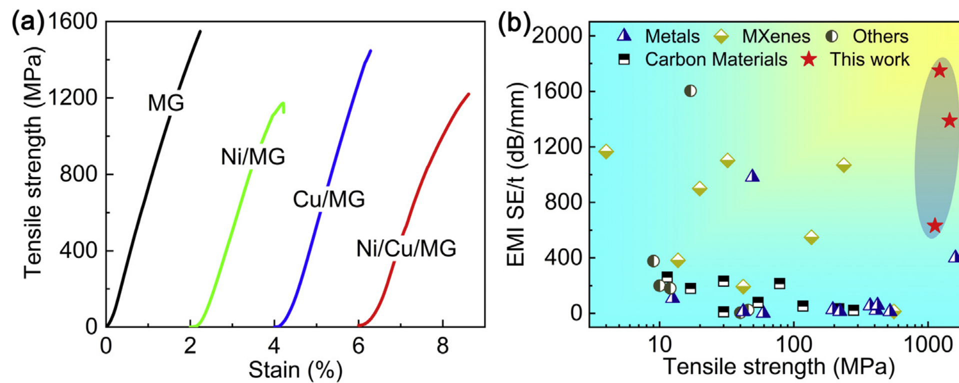

Fig. 6. (a) Stress-strain curves of MG, Ni/MG, Cu/MG and Ni/Cu/MG at a strain rate of 10^{-4} m/s. (b) EMI SE/t versus tensile strength. Metals: blue triangle; Carbon materials: black squares; MXenes: orange diamond; Others: green circle; This work: red pentagram.

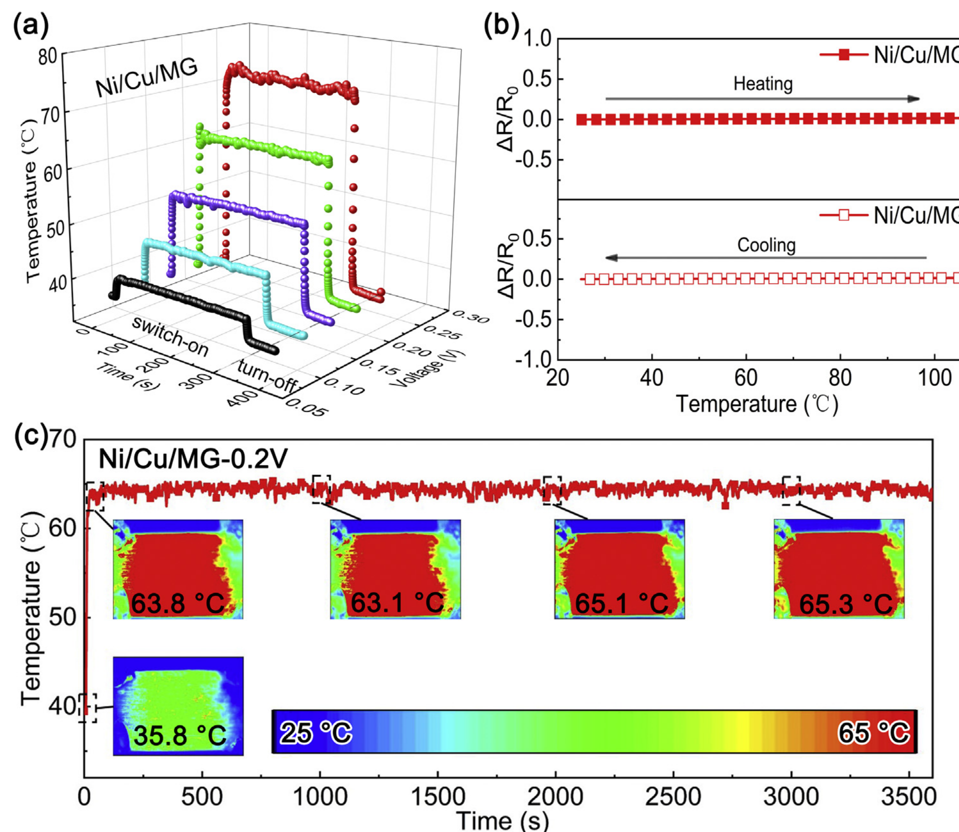

Fig. 7. Thermal management performance of Ni/Cu/MG. (a) Surface temperature as a function of time and applied voltage. (b) Variation of resistance with temperature. (c) Temperature-time curve at a constant voltage of 0.2 V. The inset in (c) displays the infrared thermal imaging photos during heating. The temperature in the inset represents the average temperature of the entire sample surface.

transferred to the surface by the ultrathin and highly conductive Cu layer [54]. In addition, Ni/Cu/MG has a high Curie temperature of 338 °C and a high crystallization temperature of 499 °C (Fig. S9), ensuring that it can be used at high temperatures for a long time. Therefore, the excellent thermal management performances, such as satisfactory Joule heating temperature under low power supply voltage, rapid response time, uniform temperature distribution, sufficient heating stability and reliability, make Ni/Cu/MG suitable for wearable thermotherapy.

4. Conclusions

In summary, this work reports a well-designed Ni/Cu/MG multilayer composite with alternate magnetic and electrical structures fabricated by facial two-step electroless plating. The Ni/Cu/MG composite displays a high EMI SE of 35 dB and a superior EMI SE/t of 1750 dB/mm at an ultrathin thickness of 0.02 mm owing to the enhancement in ohmic loss, internal absorption/reflection, and interfacial polarization loss. Moreover, the highly flexible Ni/Cu/MG composite exhibits an excellent tensile strength of 1.2 GPa and outstanding bending stability, which makes it stand out among most shielding materials. In addition, the Ni/Cu/MG composite has superior thermal management performances such as satisfactory Joule heating temperature (64 °C) at low applied voltage, fast response time (<6 s), uniform temperature distribution and sufficient stability. This work provides a simple and efficient strategy for the design of metal-based EMI shielding materials for smart and wearable electronics.

Declaration of Competing Interest

The authors report no declarations of interest.

Acknowledgements

This work was financially supported by National Key Research and Development Program of China (No. 2016YFB0300500), the National Natural Science Foundation of China (No. 51771215), the Ningbo Major Special Projects of the Plan “Science and Technology Innovation 2025” (No. 2018B10084), K.C. Wong Magna Fund in Ningbo University.

Appendix A. Supplementary data

Supplementary material related to this article can be found, in the online version, at doi:https://doi.org/10.1016/j.jmst.2020.12.012.

References

[1] P. Kumar, U. Narayan Maiti, A. Sikdar, T. Kumar Das, A. Kumar, V. Sudarsan, Polym. Rev. 59 (2019) 687–738.
[2] F. Shahzad, M. Alhabeb, C.B. Hatter, B. Anasori, S.M. Hong, C.M. Koo, Y. Gogotsi, Science 353 (2016) 1137–1140.
[3] J.J. Zhang, J.W. Li, G.G. Tan, R.C. Hu, J.Q. Wang, C.T. Chang, X.M. Wang, ACS Appl. Mater. Interfaces 9 (2017) 42192–42199.
[4] S.H. Lee, S. Yu, F. Shahzad, J.P. Hong, W.N. Kim, C. Park, S.M. Hong, C.M. Koo, Compos. Sci. Technol. 144 (2017) 57–62.
[5] P. He, X.X. Wang, Y.Z. Cai, J.C. Shu, Q.L. Zhao, J. Yuan, M.S. Cao, Nanoscale 11 (2019) 6080–6088.
[6] D. Wanasinghe, F. Aslani,Compos. Pt. B Eng. 176 (2019), 107207.
[7] J. Chen, X. Liao, W. Xiao, J. Yang, Q. Jiang, G. Li, ACS Sustain. Chem. Eng. 7 (2019) 9904–9915.
[8] M.G. Jang, S.C. Ryu, K.J. Juhn, S.K. Kim, W.N. Kim, J. Appl. Polym. Sci. 136 (2018) 47302.
[9] W.J. Long, Y.C. Gu, H. Ma, H.D. Li, F. Xing, Compos. Pt. B Eng. 168 (2019) 25–33.
[10] J. Luo, L. Wang, X. Huang, B. Li, Z. Guo, X. Song, L. Lin, L.C. Tang, H. Xue, J. Gao, ACS Appl. Mater. Interfaces 11 (2019) 10883–10894.
[11] B.A. Zhao, C.B. Park, J. Mater. Chem. C 5 (2017) 6954–6961.
[12] H. Abbasi, M. Antunes, J.I. Velasco, Prog. Mater. Sci. 103 (2019) 319–373.
[13] A. Iqbal, F. Shahzad, K. Hantanasirisakul, M.K. Kim, J. Kwon, J. Hong, H. Kim, D. Kim, Y. Gogotsi, C.M. Koo, Science 369 (2020) 446–450.
[14] A. Iqbal, P. Sambyal, C.M. Koo,Adv. Funct. Mater. 30 (2020), 2000883.
[15] S. Li, Z. Xu, Y. Dong, D. Liu, G. Sui,Compos. Pt. A Appl. Sci. Manuf. 131 (2020), 105798.
[16] S. Li, J. Li, N. Ma, D. Liu, G. Sui, ACS Sustain. Chem. Eng. 7 (2019) 13970–13980.
[17] Y. Xu, Y. Li, W. Hua, A.M. Zhang, J.J. Bao, ACS Appl. Mater. Interfaces 8 (2016) 24131–24142.
[18] K. Zhang, H.O. Yu, K.X. Yu, Y. Gao, M. Wang, J. Li, S.Y. Guo, Compos. Sci. Technol. 156 (2018) 136–143.
[19] Y.J. Tan, J. Li, Y. Gao, J. Li, S.Y. Guo, M. Wang, Appl. Surf. Sci. 458 (2018) 236–244.
[20] Y. Li, B. Shen, D. Yi, L.H. Zhang, W.T. Zhai, X.C. Wei, W.G. Zheng, Compos. Sci. Technol. 138 (2017) 209–216.
[21] Y.D. Xu, Y.Q. Yang, D.X. Yan, H.J. Duan, G.Z. Zhao, Y.Q. Liu, ACS Appl. Mater. Interfaces 10 (2018) 19143–19152.
[22] J. Yang, X. Liao, G. Wang, J. Chen, F. Guo, W. Tang, W. Wang, Z. Yan, G. Li,Chem. Eng. J. 390 (2020), 124589.
[23] A. Sheng, W. Ren, Y. Yang, D.X. Yan, H. Duan, G. Zhao, Y. Liu, Z.M. Li,Compos. Pt. A Appl. Sci. Manuf. 129 (2020), 105692.
[24] Z. Gao, Z. Jia, K. Wang, X. Liu, L. Bi, G. Wu,Chem. Eng. J. 402 (2020), 125951.
[25] C. Liang, Y. Liu, Y. Ruan, H. Qiu, P. Song, J. Kong, H. Zhang, J. Gu,Compos. Pt. A Appl. Sci. Manuf. 139 (2020), 106143.
[26] T. Hou, B. Wang, M. Ma, A. Feng, Z. Huang, Y. Zhang, Z. Jia, G. Tan, H. Cao, G. Wu,Compos. Pt. B Eng. 180 (2020), 107577.
[27] Q. Zhao, Y. Liu, E.W. Abel, Mater. Chem. Phys. 87 (2004) 332–335.
[28] G.M. Weng, J. Li, M. Alhabeb, C. Karpovich, H. Wang, J. Lipton, K. Maleski, J. Kong, E. Shaulsky, M. Elimelech, Y. Gogotsi, A.D. Taylor,Adv. Funct. Mater. 28 (2018), 1803360.
[29] D.X. Yan, H. Pang, B. Li, R. Vajtai, L. Xu, P.G. Ren, J.H. Wang, Z.-M. Li, Adv. Funct. Mater. 25 (2015) 559–566.
[30] F. Qin, H.X. Peng, Prog. Mater. Sci. 58 (2013) 183–259.
[31] B. Zhao, C.X. Zhao, R.S. Li, S.M. Hamidinejad, C.B. Park, ACS Appl. Mater. Interfaces 9 (2017) 20873–20884.
[32] K. Sushmita, T.V. Menon, S. Sharma, A.C. Abhyankar, G. Madras, S. Bose, J. Phys. Chem. C 123 (2019) 2579–2590.
[33] B. Zhao, B. Fan, G. Shao, W. Zhao, R. Zhang, ACS Appl. Mater. Interfaces 7 (2015) 18815–18823.
[34] X. Ma, Q. Zhang, Z. Luo, X. Lin, G. Wu, Mater. Des. 89 (2016) 71–77.
[35] J. Liu, H.B. Zhang, R. Sun, Y. Liu, Z. Liu, A. Zhou, Z.Z. Yu,Adv. Mater. 29 (2017), 1702367.
[36] J. Liu, Z. Liu, H.B. Zhang, W. Chen, Z. Zhao, Q.W. Wang, Z.Z. Yu,Adv. Electron. Mater. 6 (2019), 1901094.
[37] W. Chen, L.X. Liu, H.B. Zhang, Z.Z. Yu, ACS Nano 14 (2020), http://dx.doi.org/10.1021/acsnano.0c01635.
[38] Z. Ma, S. Kang, J. Ma, L. Shao, Y. Zhang, C. Liu, A. Wei, X. Xiang, L. Wei, J. Gu, ACS Nano 14 (2020) 8368–8382.
[39] R. Pandey, S. Tekumalla, M. Gupta, J. Alloys Compd. 770 (2019) 473–482.
[40] Y. Liu, X.Y. Jian, X.L. Su, F. Luo, J. Xu, J.B. Wang, X.H. He, Y.H. Qu, J. Alloys Compd. 740 (2018) 68–76.
[41] N. He, M. Liu, J. Qi, J. Tong, W. Sao, X. Yang, L. Shi, G. Tong,Chem. Eng. J. 378 (2019), 122160.
[42] S.M. Yang, Y.Y. Chang, Y.C. Hsieh, Y.J. Lee, J. Appl. Polym. Sci. 110 (2008) 1403–1410.
[43] B. Zhao, S. Zeng, X. Li, X. Guo, Z. Bai, B. Fan, R. Zhang, J. Mater. Chem. C 8 (2020) 500–509.
[44] L. Wang, X. Shi, J. Zhang, Y. Zhang, J. Gu, J. Mater. Sci. Technol. 52 (2020) 119–126.
[45] B. Zhao, R. Wang, Y. Li, Y. Ren, X. Li, X. Guo, R. Zhang, C.B. Park, J. Mater. Chem. C 8 (2020) 7401–7410.
[46] B. Zhao, Y. Li, Q. Zeng, L. Wang, J. Ding, R. Zhang, R. Che,Small 16 (2020), e2003502.
[47] B. Zhao, J. Deng, C. Zhao, C. Wang, Y.G. Chen, M. Hamidinejad, R. Li, C.B. Park, J. Mater. Chem. C 8 (2020) 58–70.
[48] Y. Yang, M. Li, Y. Wu, T. Wang, E.S. Choo, J. Ding, B. Zong, Z. Yang, J. Xue, Nanoscale 8 (2016) 15989–15998.
[49] M.M. Ahmmad, Y. Sumi, J. Mar. Sci. Technol. 15 (2009) 1–15.
[50] W. He, R. Zhang, Y. Cheng, C. Zhang, X. Zhou, Z. Liu, X. Hu, Z. Liu, J. Sun, Y. Wang, D. Qian, Z. Liu, Sci. China Mater. 63 (2020) 1318–1329.
[51] Z. Ma, S. Kang, J. Ma, L. Shao, A. Wei, C. Liang, J. Gu, B. Yang, D. Dong, L. Wei, Z. Ji, ACS Nano 13 (2019) 7578–7590.
[52] R. Zhou, P. Li, Z. Fan, D. Du, J. Ouyang, J. Mater. Chem. C 5 (2017) 1544–1551.
[53] W.L. Johnson, G. Kaltenboeck, M.D. Demetriou, J.P. Schramm, X. Liu, K. Samwer, C.P. Kim, D.C. Hofmann, Science 332 (2011) 828–833.
[54] H. Yao, Z. Zhou, L. Wang, Z. Tan, D. He, L. Zhao, Coatings 7 (2017) 173.